Identification and optical properties of axial lead centres in alkaline-earth fluorides

1989 J. Phys.: Condens. Matter 1 13

(http://iopscience.iop.org/0953-8984/1/1/002)

J. Phys.: Condens. Matter 1 (1989) 13–26. Printed in the UK

Identification and optical properties of axial lead centres in alkaline-earth fluorides

M Fockele†, F Lohse†, J-M Spaeth† and R H Bartram‡

† Fachbereich Physik, Universität-GH Paderborn, Warburger Strasse 100 A, D-4790 Paderborn, Federal Republic of Germany

‡ Department of Physics and Institute of Materials Science, University of Connecticut, Storrs, CT 06268, USA

Received 20 June 1988

Abstract. Axial Pb centres were produced by x-irradiation in Pb-doped CaF_2, SrF_2 and BaF_2, which show intense infrared emissions. One paramagnetic centre was identified by optically detected electron spin resonance (ESR) and electron–nuclear double resonance to be a Pb^+ substituting for M^{2+} (M ≡ Ca, Sr or Ba) next to an F^- vacancy along ⟨111⟩ (Pb^+ (1) centre). The absorption bands could be identified from the excitation spectrum of the infrared emission and from a combination of magneto-optical and ESR techniques. The emissions have quantum efficiencies near unity up to room temperature. The optical properties are explained by a crystal-field model analogous to that derived for the laser-active $Tl^0(1)$ centres in alkali halides. Laser action of the $Pb^+(1)$ centre is expected. Results on a $Pb^+(1)$–Pb^{2+} centre and a diamagnetic $Pb^0(2)$ centre, which are produced simultaneously, are also reported.

1. Introduction

$Tl^0(1)$ centres in alkali halides were shown to be laser active in the near infrared with attractive laser properties (Mollenauer *et al* 1982, 1983). The $Tl^0(1)$ centre consists of a neutral Tl^0 atom next to an anion vacancy along a ⟨100⟩ direction and is produced by x-irradiation of Tl-doped alkali halides at room temperature (Mollenauer *et al* 1983, Goovaerts *et al* 1981). The electronic configuration of Tl^0 is Xe $4f^{14}5d^{10}6s^26p^1$ with the ground and first excited terms of the single p electron $^2P_{1/2}$ and $^2P_{3/2}$, separated by a spin–orbit interaction of nearly 1 eV. The strong odd crystal field of the vacancy further splits and shifts the 6p manifold and partially allows electrical dipole transitions within the 6p multiplet through admixture of even-parity states. The specific interplay between the crystal field and the Tl spin–orbit interaction is the reason for the favourable laser properties (Ahlers *et al* 1984). It was therefore attempted to produce analogous $Pb^+(1)$ centres (figure 1(*a*)) with the isoelectric Pb^+ ion, which has a larger spin–orbit interaction of 1.758 eV. An appropriate lattice is that of the alkaline-earth fluorides CaF_2, SrF_2 and BaF_2. The $Pb^+(1)$ centres in these crystals appear promising with respect to good laser properties because of a strong crystal field and the large Pb^+ spin–orbit interaction. Thermal stability is one of the problems with the laser-active $Tl^0(1)$ centre in alkali halides. In alkaline-earth fluorides, better thermal stability is expected because of the

0953-8984/89/010013 + 14 $02.50

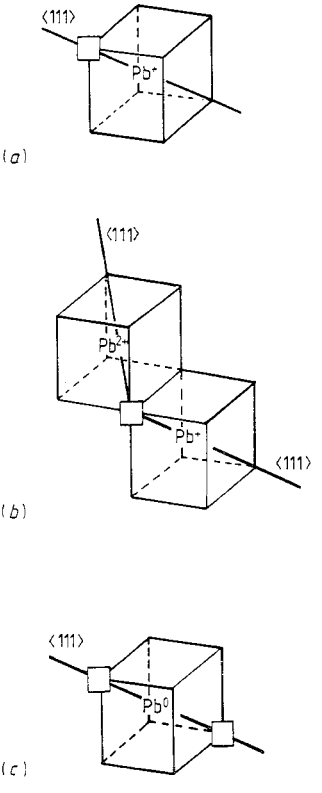

Figure 1. Pb-centre models in alkaline-earth fluorides: (*a*) $Pb^{+}(1)$ centre; (*b*) $Pb^{+}(1)$–Pb^{2+} dimer centre; (*c*) $Pb^{0}(2)$ centre.

lower mobility of anion vacancies at room temperature. Recently a $KMgF_3$ crystal doped with lead and x-irradiated at room temperature was made to lase (Hörsch and Paus 1987), where probably axial Pb^{+} centres are the laser-active defects.

In this paper, we report mainly on the production, the identification and the optical properties of $Pb^{+}(1)$ centres in CaF_2, SrF_2 and BaF_2. Apart from standard optical absorption and emission experiments, the identification was achieved by applying optical detection of electron spin resonance (ODESR) and optical detection of electron–nuclear double resonance (ODENDOR) (Ahlers *et al* 1983, Hofmann *et al* 1984). Simultaneously, two other lead centres, which both also have an intense infrared emission, are produced on x-irradiation of the alkaline-earth fluorides. They were identified as a paramagnetic $Pb^{+}(1)$–Pb^{2+} dimer centre (figure 1(*b*)) and a diamagnetic $Pb^{0}(2)$ centre, in which two vacancies along ⟨111⟩ are nearest neighbours to a substitutional Pb^{0} atom (figure 1(*c*)). The identification of the latter defect is primarily based on the theory of the infrared emission properties, which is presented in the following paper (Bartram *et al* 1989).

Finally, the optical gain of the $Pb^{+}(1)$ centres is calculated; this forecasts laser action for these defects. The optical properties of these centres are discussed in the framework of the crystal-field model derived for $Tl^{0}(1)$ centres (Goovaerts *et al* 1981). The ground-state wavefunction, which approximately explains the measured superhyperfine (SHF) interactions with the nearest F^{-} neighbours, is also discussed.

2. Experimental details

The alkaline-earth crystals were grown from Merck suprapure materials with the Bridgman technique and doped with between 0.3 and 3 mol.% of the corresponding lead fluoride. The crystals were then irradiated with x-rays (50 kV, 30 mA) at temperatures between 300 and 500 K. The highest $Pb^+(1)$ centre concentration was achieved at temperatures higher than the Debye temperature of the host crystal. The centres are stable at room temperature and do not decay under intense optical excitations. Simultaneously, other Pb centres are also formed by x-irradiation, whereby the different relative amounts of the various centres is influenced by the irradiation temperature and the Pb^{2+} concentration. The final concentration of the $Pb^0(2)$ centres decreases with higher irradiation temperature compared with $Pb^+(1)$ centres. In highly doped samples (2–3 mol.% PbF_2) x-irradiation produces the $Pb^+(1)$–Pb^{2+} dimer defect.

The optical absorption, emission, luminescence decay time and excitation measurements were performed with a computer-controlled optical spectrometer. Decay time measurements were restricted to decay times above 500 ns, the rise time of the Ge infrared detector (EO817, Northcoast). The emission quantum yield was measured relative to the quantum yield of the $Tl^0(1)$ centre in KCl (Fockele *et al* 1985). ODESR and ODENDOR measurements of the ground state were performed by monitoring the microwave- and radiofrequency-induced change in the magnetic circular dichroism (MCD) of the optical absorption bands (Ahlers *et al* 1983, Hofmann *et al* 1984). In order to determine the optical absorption bands belonging to one particular Pb centre when absorption bands of other defects are superimposed, the method of 'MCD tagged by ESR' was used. In this method, one measures a type of excitation spectrum of the ODESR lines and thus selects the MCD, which belongs to only one ESR spectrum and defect, respectively (Ahlers *et al* 1983).

3. Experimental results

3.1. Optical properties

Three infrared emission bands are excited in x-irradiated Pb-doped SrF_2, CaF_2 and BaF_2 crystals. Figure 2 shows the three infrared emission bands peaking at 1.058, 1.35 and 1.6 μm for SrF_2. Since the optical results are very similar for all three crystals, only SrF_2 will be described in detail. The optical absorption is a superposition of many bands (figure 3(*a*)) due to several defects. A separation of the bands due to each centre can be achieved by measuring the emission excitation spectrum and the MCD tagged by ESR.

The three emission bands belong to three different defects, as is seen from the excitation spectrum (figure 3(*b*)). In table 1 the corresponding optical absorption and emission data are collected.

The identification of the two paramagnetic centres was made by ODESR–ODENDOR experiments described below while the nature of the third centre was derived from an interpretation of the radiative lifetime. To facilitate the discussion, the centre identification is already stated here: the excitation spectrum, curve A in figure 3(*b*), belongs to $Pb^+(1)$ centres, curve C to $Pb^+(1)$–Pb^{2+} dimer centres and curve B to $Pb^0(2)$ centres. The emissions can each be excited in three bands; thus the absorption follows qualitatively a very similar pattern to what was found for the $Tl^0(1)$ centres in alkali halides

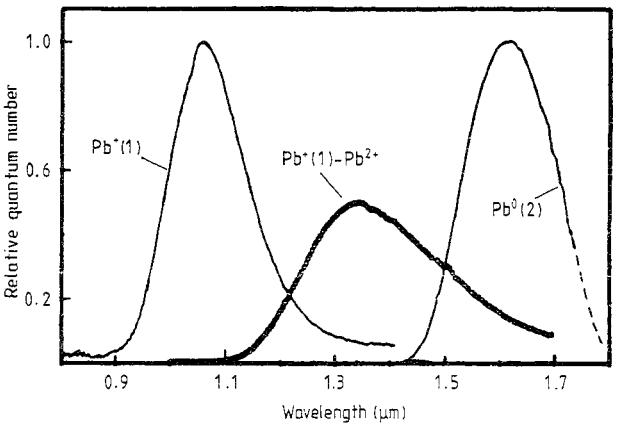

Figure 2. Optical emission spectra of SrF_2:Pb^{2+}, x-ray irradiated at 300 K and measured at 10 K. The excitation of $Pb^+(1)$ emission at 0.66 μm, $Pb^+(1)$–Pb^{2+} dimer emission at 0.74 μm and $Pb^0(2)$ emission at 1.02 μm are shown.

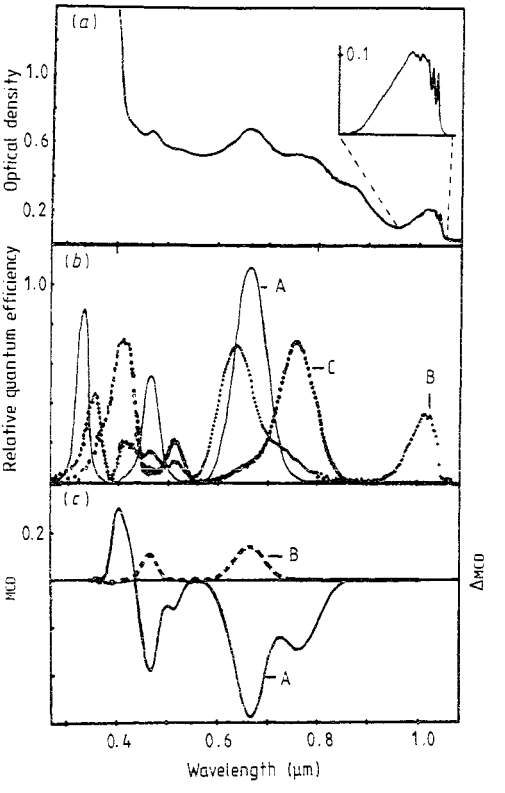

Figure 3. Optical and magneto-optical properties of $Pb^+(1)$, $Pb^0(2)$ and $Pb^+(1)$–Pb^{2+} dimer centres in SrF_2: (*a*) absorption spectrum; (*b*) excitation spectrum of the emission of the $Pb^+(1)$ centre (curve A) of the $Pb^0(2)$ centre (curve B) and of the $Pb^-(1)$–Pb^{2+} dimer centre (curve C); (*c*) MCD at 2 T and 1.8 K of $Pb^+(1)$ and $Pb^+(1)$–Pb^{2+} dimer centres (curve A) and MCD tagged by ESR of $Pb^+(1)$ centres at 1.25 T, 24 GHz and $\boldsymbol{B}_0 \parallel \langle 100 \rangle$ (curve B).

Table 1. Energies A_i of the absorption bands and the emission band E_e of $Pb^+(1)$, $Pb^+(1)$–Pb^{2+} dimer and $Pb^0(2)$ centres in alkaline-earth fluorides at 10 K. The A_1- and A_2-values for $Pb^+(1)$ were obtained from MCD tagged by ESR. The relative intensities are accurate to 0.1, and the energies of the absorption and emission bands to 5 meV. $\delta\nu_A$ and $\delta\nu_E$ are the halfwidths of the absorption and emission bands, respectively.

Centre	Crystal	A_4 (eV)	A_3 (eV)	A_2 (eV)	A_1 (eV)	$\delta\nu_A$ (meV)	E_e (eV)	$\delta\nu_E$ (meV)
$Pb^+(1)$	CaF_2		4.190	2.728	1.946	273	1.308	198
$Pb^+(1)$	SrF_2		3.707	2.653	1.866	205	1.172	189
$Pb^+(1)$	BaF_2		3.595	2.523	1.742	174	1.057	166
$Pb^+(1)$–Pb^{2+}	SrF_2			2.41	1.61	215	0.94	200
$Pb^0(2)$	SrF_2	3.56	1.97	1.22		240	0.78	95
Relative intensity		0.41	0.64	0.32				

(Ahlers *et al* 1983). Only the absorption band of the $Pb^0(2)$ centres at 1.02 μm has a resolved phonon structure with a vibronic energy of about 6 meV (see figure 3(*a*), inset), indicating a weaker electron–phonon coupling compared with the other two Pb defects.

Another clear difference between the $Pb^+(1)$ and $Pb^+(1)$–Pb^{2+} dimer centre and the $Pb^0(2)$ centre is the radiative lifetime of each centre. While the radiative lifetime at 10 K for $Pb^+(1)$-type centres is below 500 ns (more precise measurements were not possible in the infrared region), the radiative lifetime of the 1.6 μm emission of $Pb^0(2)$ centres is very much longer: 10.3 ms at 10 K and 3.3 ms at room temperature. Finally, measurements of the MCD of the absorption band (figure 3(*c*), curve A) shows that only the excitation bands A and C in figure 3(*b*) are due to paramagnetic centres, while curve B must be due to a diamagnetic defect. While the two centres giving rise to curves A and C in the excitation spectrum behave very similarly in all optical properties, the third diamagnetic centre seems to be of a different nature. Its identification will be discussed in the following paper (Bartram *et al* 1988).

3.2. Optically detected electron spin resonance

Figure 4(*b*) shows the ODESR spectrum at 24 GHz for three orientations of the magnetic field along ⟨100⟩, ⟨110⟩ and ⟨111⟩ measured in the low-energy absorption band at 0.66 μm of the $Pb^+(1)$ centres. The most intense ESR lines are due to the Pb^+ isotopes with no magnetic moment (77.4% abundance). They are accompanied by hyperfine doublets due to the nuclear spin $\frac{1}{2}$ of ^{207}Pb with 22.6% abundance in the expected intensity ratio of approximately 1:7. The complete ESR angular dependence for rotation in a (110) plane is shown in figure 4(*c*). The full curves, labelled by the eight possible different orientations of the centres, were calculated with the appropriate spin Hamiltonian for C_3 symmetry about ⟨111⟩. When keeping the resonance conditions for one ESR line for a specific crystal orientation and magnetic field value and measuring the ODESR effect as a function of the wavelength, one only measures that MCD effect which belongs to the selected orientation of the $Pb^+(1)$ centre (Ahlers *et al* 1983). This spectrum is shown in figure 3(*c*), curve B, for the resonance line at 1.25 T and for $\boldsymbol{B}_0 \| \langle 100 \rangle$, $\nu = 24$ GHz which belongs to the orientations 1–4 of the $Pb^+(1)$ centres (figure 4(*a*)). In this way, two absorption bands of the $Pb^+(1)$ centres could be unambiguously identified. They are

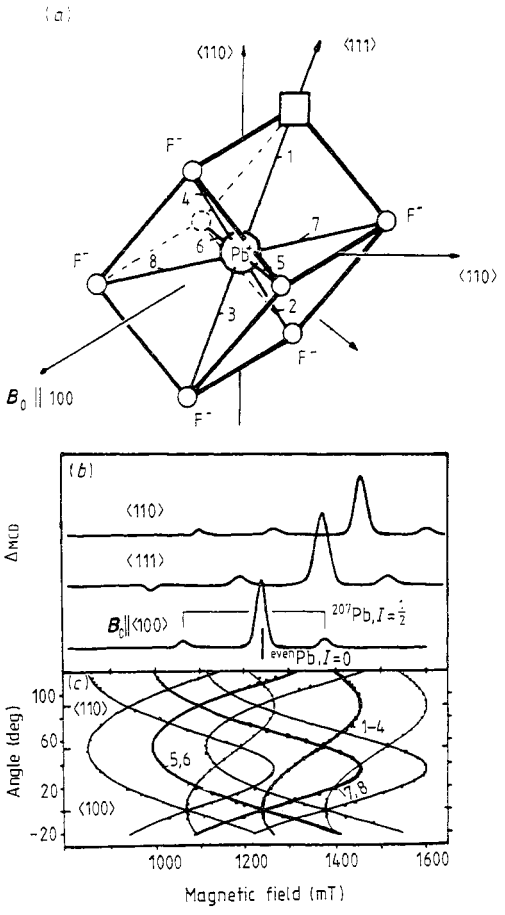

Figure 4. ODESR of $Pb^+(1)$ centres in SrF_2: (*a*) $Pb^+(1)$-centre model with the eight possible orientations of the centre; (*b*) ODESR spectra for $\boldsymbol{B}_0 \parallel \langle 100\rangle$, $\langle 110\rangle$ and $\langle 111\rangle$ measured in the 0.66 μm absorption band of the $Pb^+(1)$ centre (24 GHz; 1.8 K); (*c*) angular dependence of the ODESR spectrum for rotation of $\boldsymbol{B}_0$ in a (110) plane.

identical with the excitation bands of the 1.058 μm emission. Below 0.35 μm the MCD could not be measured.

When measuring the ODESR spectrum in the MCD band corresponding to the excitation band C in figure 3, i.e. in the lowest-energy MCD band in figure 3(*c*), a new ESR spectrum

Table 2. ESR parameters of $Pb^+(1)$ and $Pb^+(1)$–Pb^{2+} dimer centres in alkaline-earth fluorides. The *g*-values are accurate to ±0.005 and the HF interaction to ±0.5.

Centre	Crystal	g_{xx}	g_{yy}	g_{zz}	$A_{xx}=A_{yy}$ (mT)	A_{zz} (mT)
$Pb^+(1)$	CaF_2	1.191	1.191	1.703	−166.3	245.5
$Pb^+(1)$	SrF_2	1.167	1.167	1.711	−193.2	222.7
$Pb^+(1)$	BaF_2	1.036	1.036	1.634	−240.5	218.8
$Pb^+(1)$–Pb^{2+}	SrF_2	1.370	1.422	1.715	−116.6	169.3

appears, which is rather similar to that of the $Pb^+(1)$ centre, however, with different hyperfine (HF) splittings. In particular, the angular dependence cannot be explained with a fully axially symmetric g-tensor. g_{xx} and g_{yy} are slightly but clearly different. Since the centre has almost the same ⟨111⟩ character as the $Pb^+(1)$ centre and since it is produced with appreciable intensity only for highly Pb-doped samples (2–3 mol%), we conclude that it is a $Pb^+(1)$ centre slightly perturbed by a nearby Pb^{2+} ion (figure 1(*c*)). Owing to the 22.6% abundance of the magnetic ^{207}Pb isotope with $I = \frac{1}{2}$, only in 4% of all dimer centres should a further HF splitting be expected as a result of the Pb^{2+} neighbour. This could not be detected. 16% of the centres could have a small doublet hyperfine splitting from the Pb^{2+} neighbour on the ESR lines of the non-magnetic Pb isotope. This splitting is apparently too small to be resolved by ESR.

The ground-state ESR of the $Pb^+(1)$ centres could also be measured by monitoring the microwave-induced change in the magnetic circular polarisation of the emission at 1.058 μm (Mollenauer and Pan 1972). The spin polarisation of the ground state could obviously be transferred to the relaxed excited state. The ODESR spectrum obtained in this way is exactly the same as that measured with the MCD method in the $Pb^+(1)$ absorption band at 0.66 μm. Thus the correlation between absorption and emission bands of the $Pb^+(1)$ centres was confirmed once more.

3.3. Optically detected electron–nuclear double resonance of $Pb^+(1)$ centres

From the ESR spectrum alone, it cannot be decided whether the axial symmetry of the $Pb^+(1)$ centre is caused by one or two vacancies along the ⟨111⟩ direction. In order to determine the atomistic defect structure the SHF interactions with the lattice neighbours have to be determined; this could be done by performing ODENDOR experiments. Figure 5 shows a section of the ODENDOR spectrum. Many ^{19}F ENDOR lines could be observed with good signal-to-noise ratios. The angular dependence was measured under the same geometrical conditions as the ODESR spectra following the ODESR line of orientations 1–4 with no magnetic moment of the Pb^+ (figure 6(*b*)). If the centre had two vacancies, i.e. inversion symmetry, one would obtain the ^{19}F angular dependence of only one shell of six equivalent nearest ^{19}F neighbours (open circles in figure 6(*a*) below the vacancy). The angular dependence reveals, however, that there are three different ^{19}F shells of near neighbours and thus there is no inversion symmetry. The $Pb^+(1)$ centre has one nearest F site vacant along ⟨111⟩ and is therefore the analogue of the $Tl^0(1)$ centre.

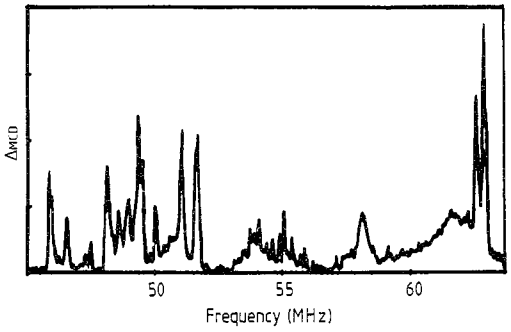

Figure 5. Section of the ODENDOR spectrum measured as radiofrequency- and microwave-induced change in the MCD of $Pb^-(1)$ centres in SrF_2 ($\lambda_{exc} = 660$ nm; 1.8 K; 24 GHz; $\boldsymbol{B}_0 \| \langle 100 \rangle = 1.25$ T).

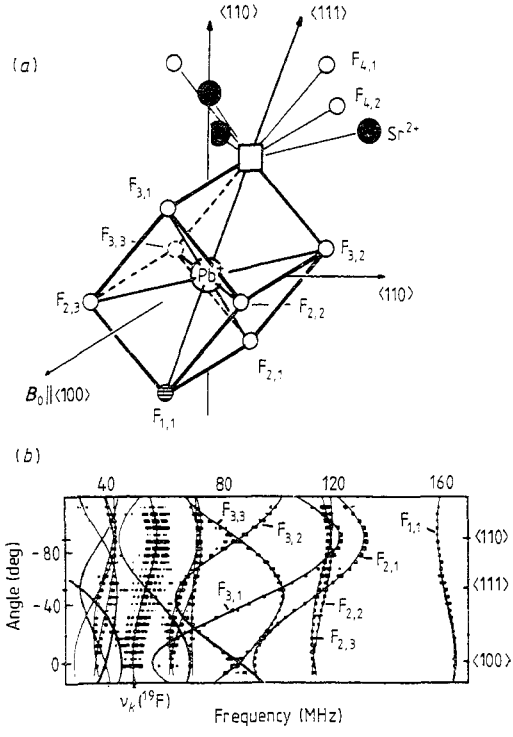

Figure 6. ODENDOR of $Pb^+(1)$ centres in SrF_2. (*a*) $Pb^+(1)$-centre model with F neighbourhood. The F are denoted by a shell number *i* and nucleus number *k* as $F_{i,k}$. (*b*) Angular dependence of ODENDOR spectra for rotation of $\boldsymbol{B}_0$ in a (110) plane measured at 0.66 μm, 24 GHz and 1.8 K, following the ESR lines of the $Pb^+(1)_{I=0}$-centre orientations 1–4 (see figure 4): ■, experimental line positions; ——, calculated angular dependences with the SHF data in table 3. $\nu_k(^{19}F)$ is the nuclear Zeeman frequency of ^{19}F.

The SHF interactions of the seven nearest ^{19}F neighbours as well as of one further F shell (figure 6(*a*), shell 4) could be determined. The full lines in figure 6(*b*) are the calculated angular dependences with the SHF data in table 3, which are given in terms of the isotropic SHF constant *a*, the anisotropic constants *b* and *b'* and the tensor angle θ,

Table 3. The SHF interactions with ^{19}F neighbours of the $Pb^+(1)$ centres in SrF_2 and BaF_2 and of F centres in SrF_2. The experimental error for the SHF constants is 0.5 MHz. θ_i are the orientations z_{SHF} measured with respect to ⟨111⟩ axes in the (110) plane. The values of *a*(F) and *b*(F) for SrF_2 are from the work of Hayes and Lambourn (1973).

Crystal	Shell	*a* (MHz)	*b* (MHz)	*b'* (MHz)	θ_i (deg)	*a*(F) (MHz)	*b*(F) (MHz)
SrF_2	1	230.7	27.6	0	0	≃0	≃0
SrF_2	2	−114.4	22.5	12.7	48.5	33.69	4.04
SrF_2	3	−45.5	42.1	25.4	−22.5	139.88	13.93
SrF_2	4	31.7	5.2	2.6	−18.9	132.50	13.53
BaF_2	1	162.5	22.1	0	0		
BaF_2	2	−85.8	25.0	19.5	47.1		
BaF_2	3	−45.2	43.9	34.1	−25.8		

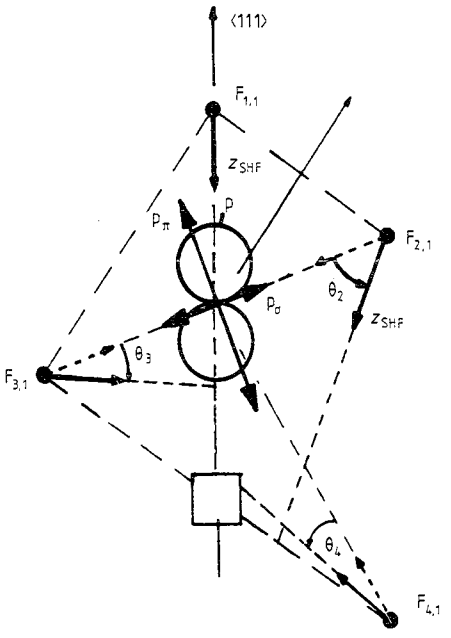

Figure 7. $Pb^+(1)$-centre model in a (110) symmetry plane of an alkaline-earth fluoride crystal with tensor axes z_{SHF} of the SHF tensors. θ_i are collected in table 3. The Pb^+ $6p_z$ orbital is indicated as well as its π and σ component with respect to shells 2 and 3.

which describes the orientation of the tensor axis with the largest interaction as shown in figure 7. The assignment of the nuclei of shells 2 and 3 to the interactions as done in table 3 cannot be justified from the experiment alone, nor can it be decided whether $a < 0, b > 0$ or $a > 0, b < 0$ from the analysis of the spectra. The choices in table 3 will be discussed in § 4.2.

4. Discussion

4.1. Optical and electron spin resonance data of the $Pb^+(1)$ centre in the crystal-field model

The optical properties and the ESR parameters of $Tl^0(1)$ centres in alkali halides could be explained rather well within a crystal-field model, in which the Tl^0 atom experiences a crystal field due to the anion vacancy. The even-parity term of the crystal-field expansion about the Tl^0 atom splits the $6p_{3/2}$ state and mixes the 6p states, while the odd-parity term admixes higher even-parity states which make optical transitions within the 6p multiplet allowed (Mollenauer *et al* 1983, Fockele *et al* 1985). This model was applied to the $Pb^+(1)$ centre. The energy levels as a function of spin–orbit splitting Δ and crystal-field parameter γ are given by (Fockele *et al* 1985)

$$E_1 = 0.5\{(\Delta - \gamma) - [(\Delta - \gamma)^2 + 8\gamma^2]^{1/2}\} \tag{1}$$

$$E_2 = 0.5\{(\Delta - \gamma) + [(\Delta - \gamma)^2 + 8\gamma^2]^{1/2}\} \tag{2}$$

$$E_3 = \Delta + \gamma. \tag{3}$$

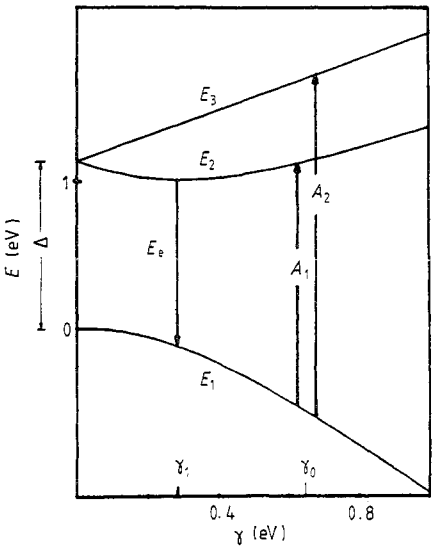

Figure 8. Energy eigenvalues E_i of the 6p manifold plotted against the crystal-field parameter γ, including the experimental absorption energies A_1 and A_2 and the emission energy E_e of $Pb^+(1)$ centres in SrF_2.

In figure 8, equations (1)–(3) are plotted for SrF_2 for the assumption, which is made also for the $Tl^0(1)$ centre, that in the crystal the spin–orbit splitting Δ is reduced compared with the free-atom value Δ_0. For $\Delta = 1.15$ eV ($\Delta_0 = 1.758$ eV) the two observed absorption bands are explained by almost the same crystal-field parameter γ_0 and the emission occurs at $\gamma_1 \simeq \frac{1}{2}\gamma_0$ for CaF_2 and SrF_2 as was observed for $Tl^0(1)$ centres. In table 4 the optical transitions are calculated for an optimal choice of γ_0, γ_1 and $\Delta = 1.15$ eV. The agreement with the experimental data (table 1) is as good as that obtained for $Tl^0(1)$ centres (Ahlers and Spaeth 1986). It should be noted that the necessary reduction in Δ of about 35% is much larger than the reduction in Δ for $Tl^0(1)$ centres of about 10% (Mollenauer *et al* 1983). Too large a Δ does not allow us to describe the optical transitions. Apparently in BaF_2 the relaxation in the excited state is larger than in the other two crystals, since $\gamma_1 \simeq \frac{1}{5}\gamma_0$.

Expressions for the g-values within the crystal-field model were derived by Goovaerts *et al* (1981):

$$g_{\parallel} = (\tfrac{2}{3}K_1^2 + \tfrac{4}{3}K_2^2 - \tfrac{4}{3}\sqrt{2}K_1K_2)f + 2(1-f) \tag{4}$$

$$g_{\perp} = |(-\tfrac{2}{3}K_1^2 + \tfrac{8}{3}K_2^2 + \tfrac{2}{3}\sqrt{2}K_1K_2)f + 2(1-f)| \tag{5}$$

Table 4. Calculation of the absorption energies A_1 and A_2 and the emission energy E_e of $Pb^+(1)$ centres in alkaline-earth fluorides with the crystal-field model for $\Delta = 1.15$ eV.

Crystal	γ_0 (eV)	γ_1 (eV)	A_1 (eV)	A_2 (eV)	E_e (eV)
CaF_2	0.70	0.37	2.02	2.64	1.305
SrF_2	0.64	0.28	1.88	2.50	1.176
BaF_2	0.59	0.12	1.76	2.34	1.080

with

$$K_1/K_2 = \tan t = -E_1/\sqrt{2}\gamma. \tag{6}$$

In the crystal-field model for the ESR data, only the 6p orbitals are included. It was necessary to introduce a localisation factor f in order to explain the $Tl^0(1)$ centre data, which expresses the fact that only the fraction f of the unpaired electron resides in the 6p orbital. The parameter t (equation (6)) is due to the mixing and normalisation of the $6p_{1/2}$ and $6p_{3/2}$ states. With the parameters f and t_g shown in table 5 a good explanation of the experimental g-values is achieved (see also table 2), as for the $Tl^0(1)$ centres (Ahlers and Spaeth 1986). The same values for f were calculated by Andriessen and Postma (1987) for CaF_2 and BaF_2 within the crystal-field model. If one determines t from the parameters Δ and γ_0 which explain the optical data according to equation (6), a different parameter t_o is obtained (table 5). This may be due to the fact that the even-parity admixtures are neglected in equations (4) and (5). Here a deficiency of the simple crystal-field model shows up.

Table 5. Theoretical values for g-factors and ^{207}Pb HF interactions for $Pb^+(1)$ centres within the crystal-field model. The parameters f, t_g and t_o are explained in the text. r_0 is the nearest-neighbour distance. $g_\parallel = g_{zz}$ and $g_\perp = g_{xx} = g_{yy}$.

Crystal	r_0 (Å)	f	t_g	t_o	$g_\parallel$	$g_\perp$	A_σ (mT)	ρ (mT)
CaF_2	2.36	0.42	18.5	39	1.706	1.190	31.1	65
SrF_2	2.50	0.43	18.5	36	1.699	1.170	4.5	64
BaF_2	2.68	0.50	18.5	34	1.640	1.033	−26.7	66

The HF interaction parameters $A_\parallel$ and $A_\perp$ and the deviations $\Delta g_\parallel$ and $\Delta g_\perp$ of the g-factors from the free-electron values can be related to each other in a crystal-field model including the spin–orbit interaction to second order (Schoemaker 1973, Nistor *et al* 1985):

$$2A_\parallel = (2 - \Delta g_\parallel)A_\sigma + (4 + 3\,\Delta g_\perp + \Delta g_\parallel)\rho \tag{7}$$

$$4A_\perp = 2(2 - \Delta g_\parallel)A_\sigma - (4 + 13\,\Delta g_\perp - 9\Delta g_\parallel)\rho. \tag{8}$$

A_σ is the isotropic HF interaction, which is the sum of the positive Fermi contact term and a negative term from exchange polarisation. ρ is the anisotropic HF interaction due to the 6p electron and should be the same for all three alkaline-earth fluorides. This is indeed found to be so (table 5). The isotropic term A_σ changes from a negative value to a positive one with decreasing vacancy–Pb^+ distance. This is qualitatively understood by the increasing crystal-field admixtures of even-parity functions such as 7s with decreasing vacancy–Pb^+ distance, which increase the Fermi contact term. These observations are very similar to those made for $Tl^0(1)$ centres in the alkali halides NaCl, KCl and RbCl (Nistor *et al* 1985).

Equations (7) and (8) do not quite hold for $Tl^0(1)$ centres because of the large spin-orbit interaction. The second-order theory is not very good. *A forteriori* this argument holds for Pb^{2+}. However, the consistency of the results obtained is surprising, where for both Tl and Pb the experimental values of $A_\parallel$ and $A_\perp$ as well as $g_\parallel$ and $g_\perp$ were used.

4.2. Superhyperfine interaction of $Pb^+(1)$ centres in SrF_2

The SHF interactions of the $Pb^+(1)$ centre show one interesting peculiarity: the isotropic and anisotropic SHF constants of shells 2 and 3 are of opposite sign, which is not observed for shells 1 and 4. Shells 2 and 3 are largely perpendicular to the Pb^+ 6p orbital, i.e. largely in a 6p nodal plane. In such a situation, there are only very small F_s and $F_{p\sigma}$ overlap admixtures to a and b, while a pronounced effect of exchange polarisation can occur, resulting mainly in a negative contribution to the isotropic interaction. Ligands in a nodal plane of 2p orbitals were observed for several O^- centres (Schirmer 1973, Stapelbroek *et al* 1976, Du Varney *et al* 1985) where large negative a-values were measured. A quantitative theory of the effect of exchange polarisation on a and b for O^- centres was recently given by Adrian *et al* (1985). In view of those observations we assigned a negative sign to a and a positive sign to b and b' for the second- and third-shell F neighbours.

If the Pb^+ 6p orbital is centred on the Sr^{2+} site as shown in figure 7, and if unpaired spin resides only in this orbital, one would expect positive a and b values for the one first-shell F neighbour and, because of their geometrical positions, the same SHF interactions for second- and third-shell neighbours. They differ, however, largely in both a- and b-values. It appears that one shell (assigned to shell 3 in table 3) contains more positive spin density than the other shell, which leads to a much smaller negative a-value and to a much larger b-value than for the second shell. A difference in a could, in principle, be explained by relaxing the Pb^+ towards the F^- vacancy. For a shift of about 22% the third-shell F^- would be in a nodal plane and could possess the large negative a-value of -114 MHz. However, then b would be smaller than the classical point dipole–dipole interaction value of 4.8 MHz (Stapelbroek *et al* 1976, Adrian *et al* 1984), which is not observed. Therefore, this cannot be an explanation for the observed SHF interactions. Another possibility is to consider that part of the unpaired electron which resides in the F^- vacancy. In a rough approximation the wavefunction could then be a superposition of a Pb^+ 6p function and a F-centre-like function. Such a possibility has already been discussed to explain the properties of $Tl^0(1)$ centres (Ahlers and Spaeth 1986). From the discussion of the ESR data (see table 5) a delocalisation of 50–60% of the unpaired electron had to be assumed. Possibly a substantial part of the wavefunction is centred at the F^- vacancy. In table 3 the experimental SHF interactions of F centres in SrF_2 are listed together with the $Pb^+(1)$ centre SHF interactions. The F-centre first-shell neighbour (shells 1a and 1b) correspond to shells 3 and 4 of the $Pb^+(1)$ centre, and their third shell to the $Pb^+(1)$ centre second shell. If one simply takes for the F-centre-like wavefunction needed here that of the F centre, about 50% localisation in the F centre would approximately explain the difference between the isotropic second- and third-shell interactions. Qualitatively, it would also result that the anisotropic third-shell SHF constant is larger than that of the second shell; also, b' is much larger for the third shell. However, the isotropic fourth-shell constant would be overestimated by a factor of about 2, while the anisotropic constant is approximately correct.

A more quantitative explanation of the SHF interactions requires better knowledge of both the Pb^+ 6p orbital and that part of the wavefunction which is centred at the vacancy. Possibly a Pb^+ 7s orbital must also be considered. The calculation of the wavefunction of $Pb^+(1)$ centres is beyond the scope of this paper.

Qualitatively, it seems clear, however, that a substantial part of the unpaired electron resides outside the Pb^+ 6p orbital in a F-centre-like wavefunction.

4.3. Laser properties of the $Pb^+(1)$ centres

An expression for the optical gain of centres was given by Mollenauer (1974). The optical gain α_0 (cm^{-1}) depends on the number N^* of excited centres obtainable, the wavelength $E_e(\mu m)$ at the luminescence band centre, the half-width $\delta\nu$ (Hz) of the emission band, the luminescence quantum efficiency η, the luminescence decay time τ_l (ns) and the refractive index n:

$$\alpha_0 = (N^* E_e^2 \eta / 8\pi n^2 \tau_l)(1/1.07\,\delta\nu). \tag{9}$$

For a net optical gain, α_0 should be well above zero to compensate for cavity losses and to provide for output of the laser. The α_0-values and the other quantities entering equation (9) for $Pb^+(1)$ centres in alkaline-earth fluorides, the Pb^+ centres in $KMgF_3$ (Hörsch and Paus 1987) and the $Tl^0(1)$ centre in KCl are collected in table 6 assuming that $N^* = 10^{16}\ cm^{-3}$. The gain of the $Pb^+(1)$ centres in alkaline-earth fluorides is about the same as for the laser-active $Tl^0(1)$ centre in KCl and Pb^+ centres in $KMgF_3$. However, the half-width is four times larger; from this it follows that there is a larger tuning range of the laser system. Judging from α_0 alone and taking into account the demonstrated laser action of Pb^+ centres in $KMgF_3$, we believe that BaF_2 or SrF_2 crystals containing $10^{16}\ cm^{-3}$ excited centres should also be laser active. The values of τ_l/η in table 6 for the $Pb^+(1)$ emission in alkaline-earth fluorides are upper estimates. Therefore the α_0-values could in fact be even larger than given in table 6.

Table 6. Optical gain for $Pb^+(1)$ and $Tl^0(1)$ centres in different hosts. The values for $KMgF_3$ are from the work of Hörsch and Paus (1987). The values of E_e, τ_l/η and $\delta\nu$ for KCl are from the work of Mollenauer *et al* (1982, 1983).

Crystal	Centre	α_0 (cm^{-1})	E_e (μm)	τ_l/η (ns)	$\delta\nu$ (10^{13} Hz)
CaF_2	$Pb^+(1)$	0.07	0.948	≈500	4.79
SrF_2	$Pb^+(1)$	0.09	1.058	≈500	4.57
BaF_2	$Pb^+(1)$	0.12	1.173	≈500	4.02
$KMgF_3$	$Pb^+(1)$	0.08	0.884	500	3.3
KCl	$Tl^0(1)$	0.15	1.503	1600	1.45

A disadvantage in the investigated $Pb^+(1)$ centre containing crystals is, however, that the absorption band of the simultaneously produced $Pb^0(2)$ centres at 1.02 μm overlaps the $Pb^+(1)$ centre emission band peaking at 1.058 μm (SrF_2). An absorption of the laser emission by the crystal itself degrades the optical gain and prevents laser action. The optical properties of $Pb^+(1)$–Pb^{2+} centres are so similar to those of the $Pb^+(1)$ centres that they may also be laser active. An advantage may be that the emission does not overlap the $Pb^0(2)$ absorption.

So far no laser action could be observed. It seems possible, however, to prevent the formation of $Pb^0(2)$ centres by an appropriate choice of Pb concentration and temperature for x-irradiation. Further attempts to observe laser action are at present under way.

5. Conclusions

The crystal-field model, which could explain the optical and ESR properties of $Tl^0(1)$ centres in alkali halides rather well, suggested the formation of $Pb^+(1)$ as laser-active centres. The properties of these centres are indeed found to be analogous and similar to those of the $Tl^0(1)$ centres. They are promising laser centres. If the formation of $Pb^0(2)$ centres can be suppressed, these crystals are expected to be attractive laser systems.

Acknowledgments

This work was supported by the Deutsche Forschungsgemeinschaft and in part by the North Atlantic Treaty Organisation under Grant RG.85/0662.

References

Adrian F J, Jette A N and Spaeth J-M 1985 *Phys. Rev.* B **31** 3923
Ahlers F J, Lohse F, Hangleiter Th, Spaeth J-M and Bartram R H 1984 *J. Phys. C: Solid State Phys.* **17** 4877
Ahlers F J, Lohse F, Spaeth J-M and Mollenauer L F 1983 *Phys. Rev.* B **28** 1249
Ahlers F J and Spaeth J-M 1986 *J. Phys. C: Solid State Phys.* **19** 4693
Andriessen J and Postma H 1987 Department of Applied Physics, Delft University of Technologie, Netherlands, private communication
Bartram R H, Fockele M, Lohse F and Spaeth J-M 1989 *J. Phys.: Condens. Matter:* 27–34
Du Varney R C, Niklas J R and Spaeth J-M 1985 *Phys. Status Solidi* b **128** 673
Fockele M, Ahlers F J, Lohse F, Spaeth J-M and Bartram R H 1985 *J. Phys. C: Solid State Phys.* **18** 1963–74
Goovaerts E, Andriessen J, Nistor S V and Schoemaker D 1981 *Phys. Rev.* B **24** 29
Hayes W and Lambourn R F 1973 *J. Phys. C: Solid State Phys.* **6**
Hofmann D, Meyer B K, Lohse F and Spaeth J-M 1984 *Phys. Rev. Lett.* **53** 1187
Hörsch G and Paus H J 1987 *Opt. Commun.* **60** 69
Mollenauer L F 1985 *The Laser Handbook* vol 4, ed. M L Stich and M Bass (Amsterdam: North Holland) ch 2, pp 143–228
Mollenauer L F and Pan S 1972 *Phys. Rev.* B **6** 772
Mollenauer L F, Vieira N and Szeto L 1982 *Opt. Lett.* **7** 414
—— 1983 *Phys. Rev.* B **27** 5332
Nistor S V, Heynderickx I, Goovaerts E, Bouwen A and Schoemaker D 1985 *Phys. Status Solidi* (b) **130** 175
Schirmer O F 1973 *J. Phys. C: Solid State Phys.* **6** 300
Schoemaker D 1973 *Phys. Rev.* B **7** 786
Stapelbroek M, Bartram R H, Gilliam O R and Madasci D P 1976 *Phys. Rev.* B **13** 1960